Journal of King Saud University – Science 33 (2021) 101645

Contents lists available at ScienceDirect

Journal of King Saud University – Science

journal homepage: www.sciencedirect.com

Original article

Analysis of Newtonian heating and higher-order chemical reaction on a Maxwell nanofluid in a rotating frame with gyrotactic microorganisms and variable heat source/sink

Yu-Ming Chu [a], Muhammad Ramzan [b,*], Naila Shaheen [b], Jae Dong Chung [c], Seifedine Kadry [d], Fares Howari [e], M.Y. Malik [f], Hassan Ali S. Ghazwani [g]

[a] Department of Mathematics, Huzhou University, Huzhou 313000, PR China
[b] Department of Computer Science, Bahria University, Islamabad 44000, Pakistan
[c] Department of Mechanical Engineering, Sejong University, Seoul 143-747, Republic of Korea
[d] Faculty of Applied Computing and Technology, Noroff University College, Kristiansand, Norway
[e] College of Natural and Health Sciences, Zayed University, 144543 Abu Dhabi, United Arab Emirates
[f] Department of Mathematics, College of Sciences, King Khalid University, Abha 61413, Saudi Arabia
[g] Department of Mechanical Engineering, Faculty of Engineering, Jazan University, 45124 Jazan, Saudia Arabia

ARTICLE INFO

Article history:
Received 21 November 2020
Revised 28 September 2021
Accepted 5 October 2021
Available online 13 October 2021

Keywords:
Maxwell nanofluid
Newtonian heating
Rotating flow
Gyrotactic microorganisms
Higher order chemical reaction

ABSTRACT

The goal of this study is to investigate the rotating Maxwell nanoliquid flow incorporating gyrotactic microbes with Newtonian heating and irregular heat source sink. The motion of the flow is induced due to linearly unidirectional elongated surface. The uniqueness of the flow is enhanced by the inclusion of additional phenomenon of higher order chemical reaction incorporated with Darcy Forchheimer flow, Fourier and Fick law. Numerical solution of the formulated problem is developed via bvp4c function in MATLAB. The influence of the embroiled parameters on the flow distribution is demonstrated through various graphs and tables. It is noticed that fluid velocity declines on incrementing the rotation parameter. An upsurge in thermal field is portrayed on augmenting the Newtonian heating. Comparative analysis of the results of the proposed model with previous published research is included which confirms the validity of the current model.

Nomenclature

Symbol	Description	Symbol	Description
$A = h_s\sqrt{\frac{v}{d}}$	Conjugate parameter for heat transfer	$K_2 = \Gamma_3 d$	Relaxation time parameter for concentration
b	Chemotaxis constant	k_c	Chemical reaction

(*continued*)

Symbol	Description	Symbol	Description
B_0	Magnetic field strength	$Lb = \frac{v}{D_n}$	Bioconvection Lewis number
C	Fluid concentration	$N_b = \frac{\tau D_B (C_w - C_\infty)}{v}$	Brownian motion parameter
C_w	Wall concentration	$N_t = \frac{\tau D_T}{v}$	Thermophoresis parameter
C_∞	Ambient concentration	Nu_x	Local Nusselt number
c_b	Drag coefficient	Nn_x	Local motile density number
c_p	Specific heat	$Pe = \frac{bw_0}{D_n}$	Bioconvection Peclet number
C_{fx}, C_{fy}	Skin friction coefficient	$\Pr = \frac{\mu c_p}{k}$	Prandtl number

(*continued on next page*)

* Corresponding author.
E-mail address: mramzan@bahria.edu.pk (M. Ramzan).

Peer review under responsibility of King Saud University.

Production and hosting by Elsevier

https://doi.org/10.1016/j.jksus.2021.101645
1018-3647/

(*continued*)

Symbol	Description	Symbol	Description
D	Space dependent source/sink parameter	Q_w	Heat flux
D_B	Brownian diffusion coefficient	Q_m	Mass flux
D_n	Diffusivity of microorganisms	Q_n	Motile flux
D_T	Thermophoretic diffusion coefficient	R	Motile microorganisms
$E = \Gamma_1 d$	Non-dimensional fluid relaxation time	$Re_x = \frac{xu_w}{\nu}$	Local Reynold number
$F = \frac{c_b}{x\sqrt{k_1}}$	Non-uniform inertia coefficient of porosity	$S_c = \frac{\nu}{D_B}$	Schmidt number
$F_r = \frac{c_b}{\sqrt{k_1}}$	Forchheimer number	Sh_x	Local Sherwood number
H	temperature dependent source/sink parameter	s	Order of reaction
$Ha = \frac{\sigma_1 B_0^2}{\rho d}$	Magnetic parameter	T	Fluid temperature
h_s	Heat transfer coefficient	T_∞	ambient temperature
k	Thermal conductivity	u, v, w	velocity component
$K_1 = \Gamma_2 d$	Relaxation time parameter for temperature	w_0	Maximum speed of swimming cell

Greek symbols

Symbol	Description	Symbol	Description
ν	Kinematic viscosity	$\delta = \frac{k_c (C_w - C_\infty)^{s-1}}{d}$	Dimensionless Chemical reaction rate
μ	Dynamic viscosity	Γ_1	Fluid moderation time
Ω	Angular velocity	σ_1	Electrical conductivity
ρ	density	σ	Bioconvection concentration difference parameter
$\alpha = \frac{\Omega}{d}$	Rotation parameter	$\tau = \frac{(\rho c_p)_s}{(\rho c_p)_f}$	Ratio between heat capacities
$\gamma = \frac{\nu}{k_1 d}$	Porosity number		

1. Introduction

Boundary layer flow over a deforming surface is immensely acknowledged by the scholars owing to its vast applications such as the, metallurgical process, glass blowing, production of rubber and plastic sheets aerodynamics, and extrusion, etc. Fluid flow on a deforming sheet was instigated by Crane (1970). Sreedevi and Reddy (2020) illustrated the behavior of chemical reaction with thermal radiation on a three-dimensional 3D Maxwell nanofluid past a deforming surface. It is observed in this investigation that by increasing the Deborah number the fluid velocity diminishes. On a Magnetohydrodynamic (MHD) Maxwell graphene nanofluid flow, the outcome of thermal radiation past a horizontal deforming surface is scrutinized by Hussain et al. (2020) in the presence of thermal slip condition. Ali et al. (2019) numerically examined Maxwell nano liquid flow on an exponential deforming surface. The impact of chemical reaction incorporated with thermal radiation is investigated by Prabhavathi et al. (2018) on a Maxwell nano liquid flow. On Maxwell nanoliquid flow Kundu et al. (2018) analyzed Cattaneo Christov (CC) model with slip effects past a nonlinear elongated surface (Table 1).

Non-Newtonian fluid flow on a stretching surface in a rotating frame has enormously been emphasized by the researchers due to its vast applications in geophysical processes and engineering and such as food treatments, disk cleaners, rotor systems, and gas turbines. Aziz et al. (2019) analytically investigated the behavior of homogeneous-heterogeneous reactions and Darcy Forchheimer on a 3D nanofluid in a rotating flow on a stretchable sheet. Shah et al. (2019) presented an analytical solution for 3D nanofluid with Cattaneo-Christov (CC) model in a rotating frame past a linearly elongated surface. It is found that by amplifying the nanoparticle fraction the fluid velocity upsurges, whereas, temperature field decays. Alzahrani et al. (2019) has discussed the impact of Darcy Forchheimer with heat generation/absorption on micropolar nano liquid between two parallel rotating plates. They found twofold flow behavior in the fluid velocity by escalating the inertia coefficient and rotating parameter. Recent studies on a Darcy Forchheimer nano liquid in a rotating outline can be seen in (Ullah et al., 2020; Hayat et al., 2019; Shafiq et al., 2020; Ramaiah et al., 2020; Hayat et al., 2020).

Non-uniform heat source and sink has broad range of applications which includes unrefined oil extraction, cooling of metal sheets and radial diffusers. The impact of irregular heat source/sink, Joule dissipation is explored by Thumma and Mishra (2020) on a 3D Eyring-Powell nanofluid on a deformable surface. Jakati et al. (2019) illustrated the effect of irregular heat on a 2D Maxwell nanofluid on a linear stretchable surface. On a micropolar fluid flow second order velocity slip amalgamated with irregular heat source sink is investigated by Kumar et al. (2019) past an elongated sheet. Khan et al. (2018) studied the impact of Darcy Forchheimer on a micropolar nanofluid in a rotating flow between two parallel plates.

A minuscule organism is considered as microscopic organisms (microorganisms) as it can be perceived via an optical microscope. They are found everywhere like in water, air, soil, rocks, plants, animals, and even in the human body. Cholera, meningitis, anthrax, citrus canker, and tuberculosis are a few diseases caused by microorganisms. Gyrotactic microorganisms are those organisms that move in stagnant water against gravity and depend on the type of species. Due to the random movement of microorganisms, the phenomenon of bio-convection arises. This micro-organisms characteristic is used in biotechnology, sedimentary basin, bioreactors, biosensors, separation of non-living and living cells. Abbasi et al. (2020) numerically analyzed Brownian motion, thermophoresis effect, and impact of bio-convection on Maxwell nanofluid past a linear deforming sheet. The effect of gyrotactic microorganisms with thermal radiation is analytically addressed by Ahmad et al. (2020) on a three-dimensional (3D) Maxwell nano-

Table 1
Depicts a comparison of the contemporary studies in the same domain for the uniqueness of the existing model.

Authors	3D flow	Variable heat source/sink	Darcy Forchheimer flow	Gyrotactic microorganisms	Rotating frame	Newtonian heating
Hayat et al. (2019)	Yes	No	Yes	No	Yes	No
Shafiq et al. (2020)	Yes	No	Yes	No	Yes	No
Sohail et al. (2020)	Yes	No	No	Yes	No	No
Ramzan (2015)	Yes	No	No	No	No	Yes
Present	Yes	Yes	Yes	Yes	Yes	Yes

fluid on an oscillatory deforming surface. Khan and Nadeem (2020) exhibited the aftermath of the magnetic field with viscous dissipation and chemical reaction on Maxwell nano liquid past an exponentially extending surface with variable slip conditions. Sohail et al. (2020) focused on gyrotactic microorganisms with homogeneous – heterogeneous reactions on a Maxwell nano liquid over a stretchable sheet incorporated with heat generation/absorption effects.

Transmission of heat and mass incorporated with chemical reaction has widespread applications such as food processing, destruction of harvests due to freezing, paper manufacturing and ceramics. Narender et al. (2020) numerically illustrated viscous dissipation on an incompressible 2D nanofluid flow on a linear elongated surface with chemical reaction. Ibrahim and Negera (2020) numerically inspected the impact of stagnation point flow on a Magnetohydrodynamic (MHD) upper convected Maxwell fluid with chemical reaction along a deforming surface. On an unsteady chemically reactive viscous flow Ijaz et al. (2020) addressed Joule heating and activation energy in a rotating frame on a stretchable sheet. On a chemically reactive Maxwell nanoliquid flow Khan et al. (2019) numerically examined the behavior of Cattaneo-Christov model over a deformable sheet.

Great amount of research is done on a rotating flow past a linear extending surface. The study of MHD Maxwell nanofluid influenced by gyrotactic microorganisms and higher-order chemical reaction in a rotating flow is still scarce and yet not discussed in the literature. The uniqueness of the problem is exacerbated by the combined effect of Newtonian heating and variable heat source/sink. MATLAB built-in function bvp4c is used to solve the specified mathematical problem. The influence of the pertinent parameters on the present analysis is illustrated graphically. The following questions are the aim of the research.

i. What is the influence of augmenting the fluid relaxation and rotation parameter on the fluid velocity?
ii. What effect does the conjugate parameter have on the thermal field?
iii. What is the aftermath of order of chemical reaction on the fluid concentration?
iv. Impact of Peclet number on the motile density profile?

2. Problem formulation

3D Darcy Forchheimer rotating flow of MHD Maxwell nanoliquid is examined on a stretchable linear surface with Newtonian heating. The sheet deforms in the x – direction. The surface is associated in the xy – planeand the fluid is considered at $z \geqslant 0$ (Fig. 1). The fluid spins about the z – axiswith constant angular velocity Ω. The effect of higher order chemical reaction, gyrotactic microbes incorporated with variable heat source and sink are additional phenomenon to enhance the uniqueness of the flow. The characteristics of Fourier and Fick law are inspected.

The innovative model is regulated by the following system of equations (Shafiq et al., 2020; Ramaiah et al., 2020):

$$\partial_x u + \partial_y v + \partial_z w = 0, \tag{1}$$

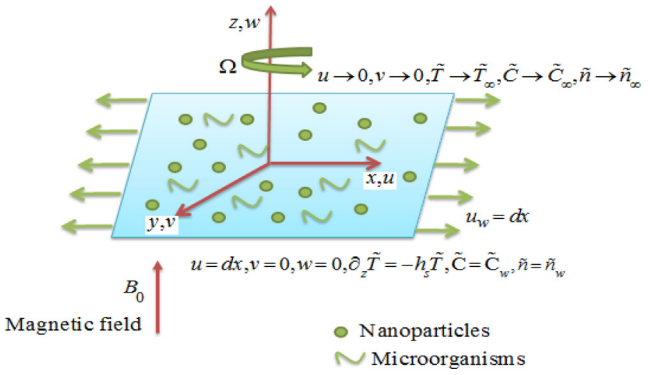

Fig. 1. Flow configuration of the model.

$$\begin{aligned} &u\partial_x u + v\partial_y u + w\partial_z u = \nu\,\partial_{zz}u - \tfrac{\sigma_1 B_0^2}{\rho}(u + \Gamma_1 w\partial_z u)\\ &+2\Omega v - \Gamma_1\begin{bmatrix} u^2\partial_{xx}u + v^2\partial_{yy}u + w^2\partial_{zz}u \\ +2(uv\partial_{xy}u + vw\partial_{yz}u + uw\partial_{xz}u) \\ -2\Omega(u\partial_x v + v\partial_y v + w\partial_z v) + 2\Omega(v\partial_x u - u\partial_y u)\end{bmatrix}\\ &-\tfrac{\nu}{k_1}u - Fu^2, \end{aligned} \tag{2}$$

$$\begin{aligned} &u\partial_x v + v\partial_y v + w\partial_z v = \nu\,\partial_{zz}v - \tfrac{\sigma_1 B_0^2}{\rho}(v + \Gamma_1 w\partial_z v)\\ &-2\Omega u - \Gamma_1\begin{bmatrix} u^2\partial_{xx}v + v^2\partial_{yy}v + w^2\partial_{zz}v \\ +2(uv\partial_{xy}v + vw\partial_{yz}v + uw\partial_{xz}v) \\ -2\Omega(u\partial_x u + v\partial_y u + w\partial_z u) \\ +2\Omega(v\partial_x v - u\partial_y v)\end{bmatrix}\\ &-\tfrac{\nu}{k_1}v - Fv^2, \end{aligned} \tag{3}$$

$$\begin{aligned} &u\partial_x\tilde{T} + v\partial_y\tilde{T} + w\partial_z\tilde{T} = \frac{k}{\rho c_p}\partial_{zz}\tilde{T} + \tau\begin{bmatrix} D_B\left(\partial_z\tilde{T}\,\partial_z\tilde{C}\right) \\ +\frac{D_T}{\tilde{T}_\infty}\left(\partial_z\tilde{T}\right)^2\end{bmatrix}\\ &-\Gamma_2\begin{bmatrix} u^2\partial_{xx}\tilde{T} + v^2\partial_{yy}\tilde{T} + w^2\partial_{zz}\tilde{T} \\ +2\left(uv\partial_{xy}\tilde{T} + vw\partial_{yz}\tilde{T} + uw\partial_{zx}\tilde{T}\right) \\ +\partial_x\tilde{T}\,(u\partial_x u + v\partial_y u + w\partial_z u) \\ +\partial_y\tilde{T}\,(u\partial_x v + v\partial_y v + w\partial_z v) \\ +\partial_z\tilde{T}\,(u\partial_x w + v\partial_y w + w\partial_z w)\end{bmatrix} + \frac{q^*}{\rho c_p}, \end{aligned} \tag{4}$$

$$\begin{aligned} &u\partial_x\tilde{C} + v\partial_y\tilde{C} + w\partial_z\tilde{C} = D_B\left(\partial_{zz}\tilde{C}\right) + \frac{D_T}{\tilde{T}_\infty}\left(\partial_{zz}\tilde{T}\right)\\ &-\Gamma_3\begin{bmatrix} u^2\partial_{xx}\tilde{C} + v^2\partial_{yy}\tilde{C} + w^2\partial_{zz}\tilde{C} \\ +2\left(uv\partial_{xy}\tilde{C} + vw\partial_{yz}\tilde{C} + uw\partial_{zx}\tilde{C}\right) \\ +\partial_x\tilde{C}\,(u\partial_x u + v\partial_y u + w\partial_z u) \\ +\partial_y\tilde{C}\,(u\partial_x v + v\partial_y v + w\partial_z v) \\ +\partial_z\tilde{C}\,(u\partial_x w + v\partial_y w + w\partial_z w)\end{bmatrix} - k_c\left(\tilde{C} - \tilde{C}_\infty\right)^s, \end{aligned} \tag{5}$$

$$u\partial_x \tilde{n} + v\partial_y \tilde{n} + w\partial_z \tilde{n} = D_n \partial_{zz} \tilde{n} - \frac{bw_0}{\left(\tilde{C}_w - \tilde{C}_\infty\right)}\left(\partial_z \tilde{n}\,\partial_z \tilde{C} + \tilde{n}\,\partial_{zz} \tilde{C}\right), \tag{6}$$

in equation (4) q^* is variable heat source/sink (Alghamdi et al., 2021)

$$q^* = \frac{ku_w}{xv}\left(\frac{D\tilde{T}_\infty u}{u_w} + H\left(\tilde{T} - \tilde{T}_\infty\right)\right) \tag{7}$$

with boundary conditions

$$u = dx,\ v = 0,\ w = 0,\ \partial_z \tilde{T} = -h_s \tilde{T},\ \tilde{C} = \tilde{C}_w,\ \tilde{n} = \tilde{n}_w \text{ at } z = 0$$

$$u \to 0,\ v \to 0,\ \tilde{T} \to \tilde{T}_\infty,\ \tilde{C} \to \tilde{C}_\infty,\ \tilde{n} \to \tilde{n}_\infty \text{ as } z \to \infty \tag{8}$$

Using appropriate transformation (Aziz et al., 2019; Sohail et al., 2020; Ramzan and Yousaf, 2015):

$$u = dxf'(\zeta), v = dxj(\zeta), w = -(dv)^{1/2} f(\zeta), \zeta = \left(\tfrac{d}{v}\right)^{1/2} z,$$
$$\tilde{T} = \tilde{T}_\infty \theta(\zeta) + \tilde{T}_\infty,\ \tilde{C} = \left(\tilde{C}_w - \tilde{C}_\infty\right)\phi(\zeta) + \tilde{C}_\infty,\ \tilde{n} = \left(\tilde{n}_w - \tilde{n}_\infty\right)R(\zeta) + \tilde{n}_\infty. \tag{9}$$

By utilizing the above transformation equation (1) is trivially equated. However, equations (2) - (6) and (8) take the form:

$$\begin{aligned} &\tfrac{d^3 f}{d\zeta^3} + f\tfrac{d^2 f}{d\zeta^2} - (1+F_r)\left(\tfrac{df}{d\zeta}\right)^2 + 2\left(\alpha j - \alpha Ef\tfrac{dj}{d\zeta} + Ef\tfrac{df}{d\zeta}\tfrac{d^2 f}{d\zeta^2}\right) - Ef^2\tfrac{d^3 f}{d\zeta^3} \\ &\quad -(Ha^2+\gamma)\tfrac{df}{d\zeta} \\ &\quad +Ha^2 Eff'' = 0, \end{aligned} \tag{10}$$

$$\begin{aligned} &\tfrac{d^2 j}{d\zeta^2} + 2\left(Ef\tfrac{df}{d\zeta}\tfrac{dj}{d\zeta} + \alpha E\left(\left(\tfrac{df}{d\zeta}\right)^2 - f\tfrac{d^2 f}{d\zeta^2}\right) - \alpha\left(\tfrac{df}{d\zeta} + Ej^2\right)\right) - (Ha^2+\gamma)j \\ &\quad -Ef^2\tfrac{d^2 j}{d\zeta^2} + f\tfrac{dj}{d\zeta} - \tfrac{df}{d\zeta}j + Ha^2 Ef\tfrac{dj}{d\zeta} \\ &\quad -F_r j^2 = 0, \end{aligned} \tag{11}$$

$$\frac{d^2\theta}{d\zeta^2} + \Pr\left(f\frac{d\theta}{d\zeta} + N_b\frac{d\theta}{d\zeta}\frac{d\phi}{d\zeta} + N_t\left(\frac{d\theta}{d\zeta}\right)^2 - K_1\left(f^2\frac{d^2\theta}{d\zeta^2} + f\frac{df}{d\zeta}\frac{d\theta}{d\zeta}\right)\right) + D\frac{df}{d\zeta} + H\theta = 0, \tag{12}$$

$$\frac{d^2\phi}{d\zeta^2} + N_t.\frac{1}{N_b}\frac{d^2\theta}{d\zeta^2} - S_c\left(\delta\phi^s - f\frac{d\phi}{d\zeta} + K_2\left(f^2\frac{d^2\phi}{d\zeta^2} + f\frac{df}{d\zeta}\frac{d\phi}{d\zeta}\right)\right) = 0, \tag{13}$$

$$\frac{d^2 R}{d\zeta^2} - Pe\left(\frac{d\phi}{d\zeta}\frac{dR}{d\zeta} + (R+\sigma)\frac{d^2\phi}{d\zeta^2}\right) + Lbf\frac{dR}{d\zeta} = 0, \tag{14}$$

and

$$\begin{aligned} &\text{At } \zeta = 0\ f(\zeta) = 0,\ \tfrac{df}{d\zeta} = 1,\ j(\zeta) = 0,\ \tfrac{d\theta}{d\zeta} = -A(1+\theta(\zeta)),\ \phi(\zeta) = 1,\ R(\zeta) = 1 \\ &\text{As } \zeta \to \infty\ \tfrac{df}{d\zeta} \to 0,\ j(\zeta) \to 0,\ \theta(\zeta) \to 0,\ \phi(\zeta) \to 0,\ R(\zeta) \to 0 \end{aligned} \tag{15}$$

The mathematical forms of surface drag force, temperature gradient are specified as:

$$C_{fx} = \frac{\tau_{wx}}{\rho u_w^2}$$

$$\tau_{wx} = \mu(1+E)\partial_z u|_{z=0} \tag{16}$$

$$C_{fy} = \frac{\tau_{wy}}{\rho u_w^2}$$

$$\tau_{wy} = \mu(1+E)\partial_z v|_{z=0} \tag{17}$$

$$Nu_x = \frac{xQ_w}{k(\tilde{T} - \tilde{T}_\infty)}$$

$$Q_w = -k\partial_z \tilde{T}\Big|_{z=0} \tag{18}$$

By utilizing equation (9), equation (16) - (18) are transmuted as:

$$C_{fx}(Re_x)^{0.5} = (1+E)\frac{d^2 f}{d\zeta^2}\Big|_{\zeta=0} \tag{19}$$

$$C_{fy}(Re_y)^{0.5} = (1+E)\frac{dj}{d\zeta}\Big|_{\zeta=0} \tag{20}$$

$$Nu_x(Re_x)^{-0.5} = -\frac{d\theta}{d\zeta}\Big|_{\zeta=0} \tag{21}$$

3. Numerical solution

Numerous analytical, exact and numerical techniques (Xia et al., 2021; Wakif et al., 2021; Rasool and Wakif, 2021; Wakif et al., 2021; Wakif et al., 2020; Alghamdi et al., 2021; Thumma et al., 2020; Shaheen et al., 2021; Wakif and Sehaqui, 2020; Chen et al., 2021) can be used to solve the system of ODEs. The exact solution of highly nonlinear coupled system of ODEs (10)-(14), with the boundary conditions (15) is not possible. Numerical solution of the flow model is computed via bvp4c function in MATLAB. The numerical procedure is given below:

$$\begin{aligned} &f = Y_1, f' = Y_2, f'' = Y_3, f''' = Y_3' = YY_1, j = Y_4, j' = Y_5, j'' = Y_5' = YY_2, \\ &YY_1 = \tfrac{1}{(1-E.Y_1^2)}\left[-Y_1.Y_3 + (1+F_r)Y_2^2 - 2(\alpha.Y_4 - \alpha.E.Y_1.Y_5 + E.Y_1.Y_2.Y_3) + (Ha+\gamma)Y_2\right], \\ &YY_2 = \tfrac{1}{(1-E.Y_1^2)}\begin{bmatrix} -2\left(E.Y_1.Y_2.Y_5 + \alpha.E\left(Y_2^2 - Y_1.Y_3\right) - \alpha\left(Y_2 + E.Y_4^2\right)\right) \\ -Y_1.Y_5 + Y_2.Y_4 + (Ha+\gamma)Y_4 + F_r.Y_4^2 \end{bmatrix}, \\ &\theta = Y_6, \theta' = Y_7, \theta'' = Y_7' = YY_3, \phi = Y_8, \phi' = Y_9, \phi'' = Y_9' = YY_4, \\ &YY_3 = \tfrac{1}{(1-K_1.Y_1^2.\Pr)}\left[-\Pr\left(Y_1.Y_7 + N_b.Y_7.Y_9 + N_t.Y_7^2 - K_1Y_1.Y_2.Y_7\right) - D.Y_2 - H.Y_6\right], \\ &YY_4 = \tfrac{1}{(1-S_c.K_2.Y_1^2)}\left[\left(-\tfrac{N_t}{N_b}\right).YY_3 + S_c\left(\delta(Y_8)^s - Y_1.Y_9 + K_2Y_1.Y_2.Y_9\right)\right], \\ &R = Y_{10}, R' = Y_{11}, R'' = Y_{11}' = YY_5, \\ &YY_5 = Pe\left[\phi'R' + (R+\sigma)\phi''\right] - Lb.f.R \\ &\text{and the boundary conditions are} \\ &\text{At } \zeta = 0\ Y_1(0) = 0, Y_2(0) = 1, Y_4(0) = 0, Y_7(0) = -A.(1+Y_6(0)), Y_8(0) = 1, Y_{10}(0) = 1 \\ &\text{As } \zeta \to \infty\ Y_2(\infty) \to 0, Y_4(\infty) \to 0, Y_6(\infty) \to 0, Y_8(\infty) \to 0, Y_{10}(\infty) \to 0 \end{aligned} \tag{22}$$

4. Graphical analysis

The main focus of this section is to explore the impact of various physical factors on involved profiles. For the graphical analysis of the non-dimensional parameters following numerical values are taken

$0.1 \leqslant E \leqslant 0.6, 0.1 \leqslant Ha \leqslant 0.5, 0.2 \leqslant \gamma \leqslant 0.4, 0.1 \leqslant F_r \leqslant 0.5$,- $0.1 \leqslant \alpha \leqslant 0.3$, $0.1 \leqslant K_1 \leqslant 0.5$,

$0.1 \leqslant N_b \leqslant 0.3, 0.1 \leqslant N_t \leqslant 0.3, 0.1 \leqslant D \leqslant 0.3, 0.1 \leqslant H \leqslant 0.3$, $0.1 \leqslant K_2 \leqslant 0.5, 0.5 \leqslant S_c \leqslant 1.2$,

$0.3 \leqslant \delta \leqslant 0.7, 0.1 \leqslant A \leqslant 0.3, 1 \leqslant s \leqslant 3, 0.5 \leqslant Pe \leqslant 0.9, 0.1 \leqslant \sigma \leqslant 0.5$, $0.6 \leqslant Lb \leqslant 1$.

Figs. 2 & 3 depicts the behavior of $x-$component velocity $f'(\zeta)$and $y-$componentof velocity $j(\zeta)$. The behavior of numerous values of non-dimensional fluid relaxation time Eon $f'(\zeta)$ and $j(\zeta)$ is illustrated in Figs. 2(a) and 2(b). Fig. 2(a) percepts that as Ehas direct proportionate to fluid moderation time Γ_1. By augmenting E, fluid moderation time boosts which halts the fluid flow. Eventually, it is perceived that$f'(\zeta)$drops. Fig. 2(b) shows that on incrementing the fluid relaxation time $j(\zeta)$increases adjacent to the wall, while it decreases in magnitude away from the wall. Negative values of $j(\zeta)$ exhibits that flow due to rotational effect is only in the direction of y' - axis. The impact of rotation parameter α on the velocity field is deliberated in Figs. 3(a) and 3(b). Since $\alpha = \frac{\Omega}{d}$, so by augmenting α angular velocity increases. The fluid is rotating and flowing. By enlarging $\alpha$the rotation rate increases in contrast to the stretching rate. Therefore, $f'(\zeta)$ decreases as the motion of the fluid slow down. Fig. 3(a) shows that $f'(\zeta)$is dwindling function of α. Fig. 3(b) exhibits an oscillatory configuration for escalating values of α. The rotation parameter plays a major role in accelerating the flow in$y-$direction. It is seen that $j(\zeta)$ descends and the fluid accelerates in the y-direction.

The impression of conjugate parameter A on thermal field $\theta(\zeta)$ is portrayed in Fig. 4. The rate of heat transmission is accelerated on augmenting$A$. This is due to the transfer of heat from the heated surface to the cold fluid. This elevates $\theta(\zeta)$. The outcome of variable source and sink parameter on $\theta(\zeta)$is sketched in Figs. 5(a)-5(d). Growing values of $D\&H$ i.e$D > 0, H > 0$corresponds to irregular heat source implying that more heat is generated. Thus, an upsurge is noticed in $\theta(\zeta)$. Influence of irregular heat sink i.e $D < 0, H < 0$ is shown in Figs. 5(c) & 5 (d) corresponds to absorption of heat. Therefore, thermal field deteriorates. Fig. 6 portrays the effect of growing values of higher-order reaction s on $\phi(\zeta)$. By upsurging s, the rate of mass transfer is enhanced. Hence, $\phi(\zeta)$rises. Variation of Peclet number on motile density profile is portrayed in Fig. 7.

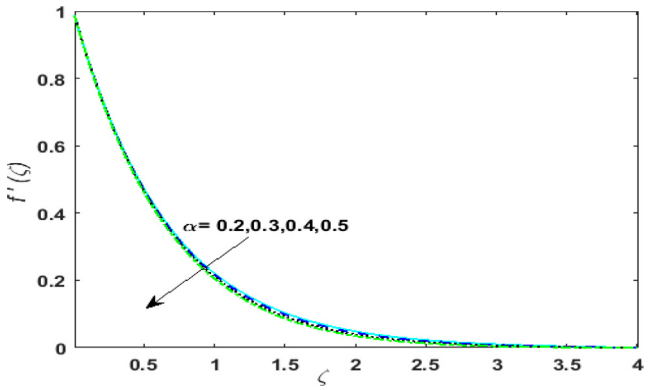

Fig. 3a. Behavior of rotation parameter on $f'(\zeta)$.

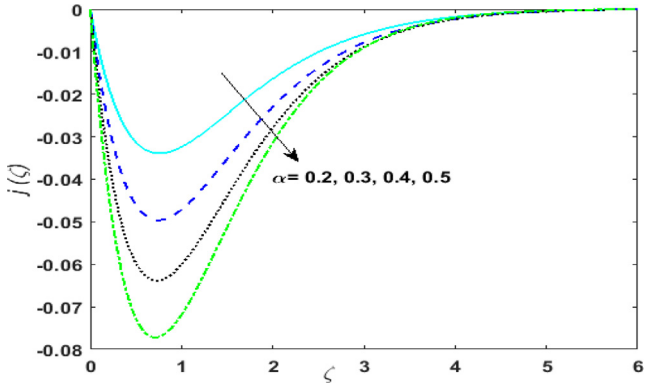

Fig. 3b. Behavior of rotation parameter on $j(\zeta)$.

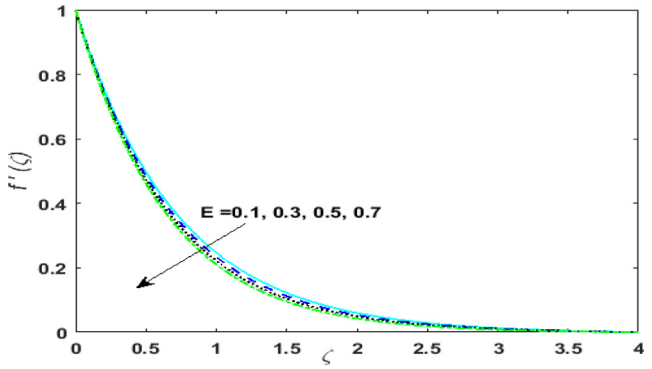

Fig. 2a. Impact of fluid relaxation time on $f'(\zeta)$.

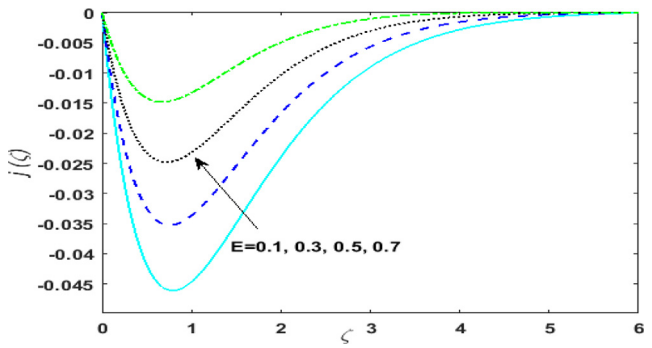

Fig. 2b. Impact of fluid relaxation time on $j(\zeta)$.

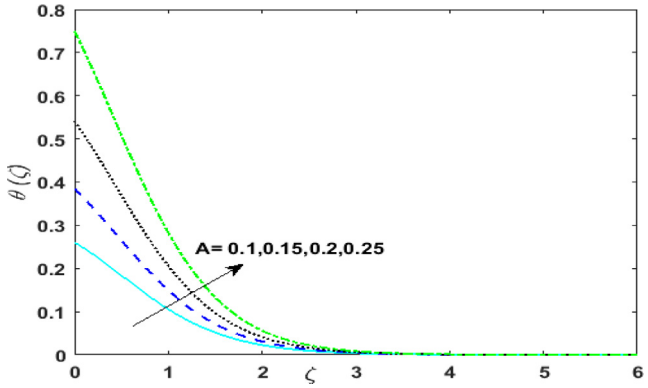

Fig. 4. Behavior of conjugate heat parameter on $\theta(\zeta)$.

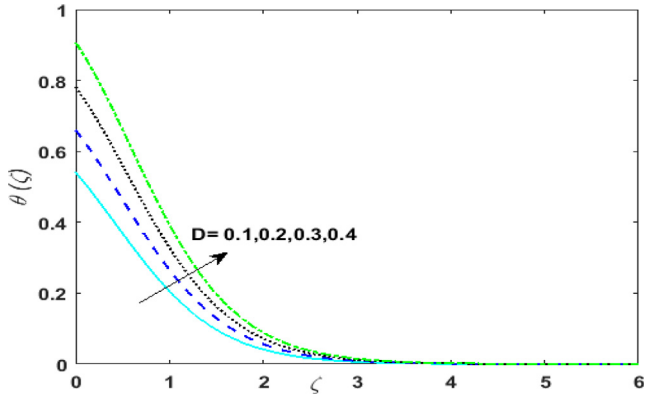

Fig. 5a. Impact of variable space dependent source parameter $D > 0$ on $\theta(\zeta)$.

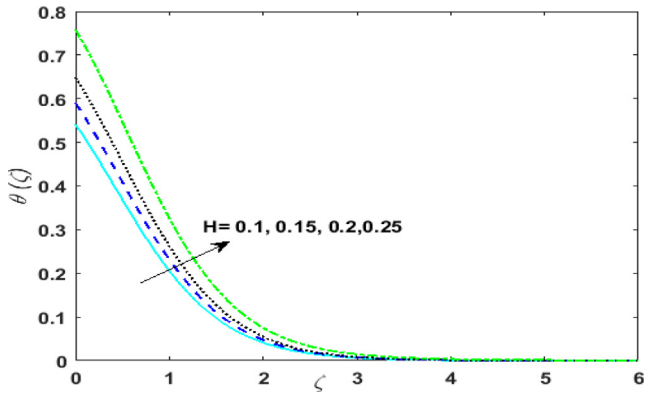

Fig. 5b. Impact of variable temperature dependent source parameter $H > 0$ on $\theta(\zeta)$.

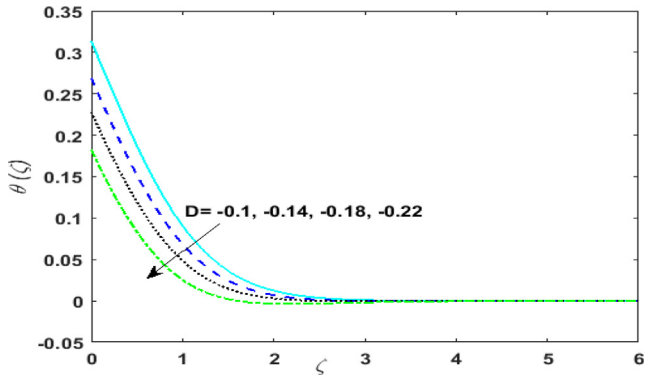

Fig. 5c. Impact of variable space dependent sink parameter $D < 0$ on $\theta(\zeta)$.

On incrementing Peclet number diffusion of microorganisms decreases. Hence, motile density of fluid diminishes. The impact of A, K_1, Eon local Nusselt number is described in Table 2. It is noticed that by increasing A and K_1 the rate of heat transfer enhances. However, $Nu_x Re_x^{-0.5}$decays for larger values of E. Table 3 shows an outstanding correlation of the current outcome for the rotation parameter with Nazar et al. (2004), Wang (1988), and Ali et al. (2020).

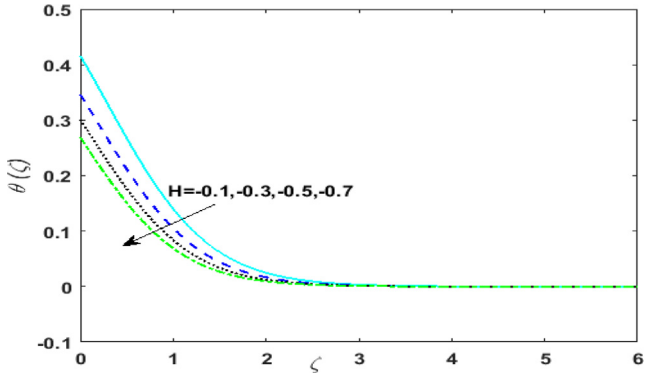

Fig. 5d. Impact of variable temperature dependent sink parameter $H < 0$ on $\theta(\zeta)$.

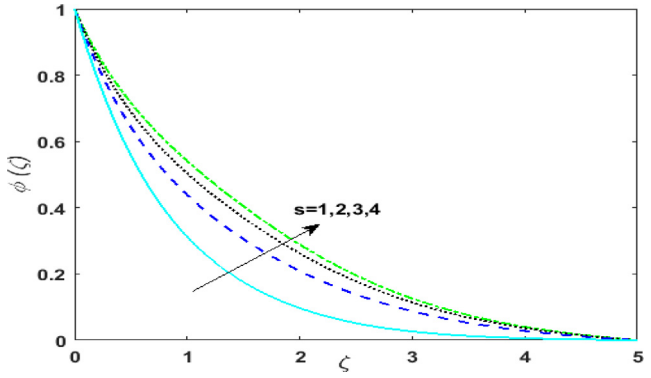

Fig. 6. Outcome of higher order reaction on $\phi(\zeta)$.

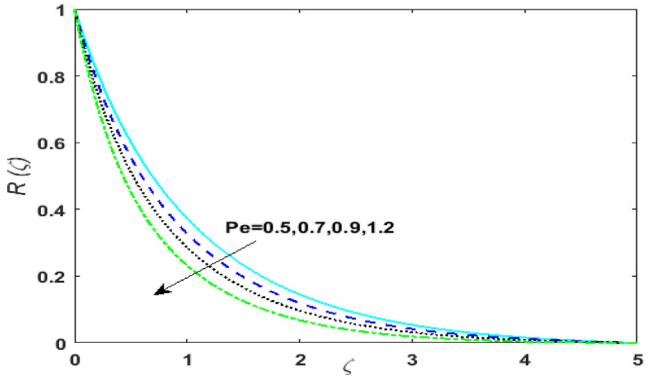

Fig. 7. Outcome of Peclet number on $R(\zeta)$.

Table 2
Computational values of $Nu_x Re_x^{-0.5}$ against different estimation of A, K_1, E.

A	K_1	E	$Nu_x Re_x^{-0.5}$
0.1			0.1241273
0.2			0.2962659
0.3			0.5595729
	0.6		0.1297434
	0.7		0.12980309
	0.8		0.12986562
		0.5	0.13087804
		0.6	0.1295171
		0.7	0.1264253

Table 3
An outstanding correlation of the current outcome for the rotation parameter α with Nazar (2004), Wang (1988) and Ali (2020).

α	Nazar (2004)		Wang (1988)		Ali (2020)		Present	
	$-f''(0)$	$-j'(0)$	$-f''(0)$	$-j'(0)$	$-f''(0)$	$-j'(0)$	$-f''(0)$	$-j'(0)$
0	1	0	1	0	1	0	1	0
0.5	1.1384	0.5128	1.1384	0.5128	1.13844	0.51283	1.13848	0.51268
1	1.3250	0.8371	1.3250	0.8371	1.32501	0.83715	1.32501	0.83712
2	1.6523	1.2873	1.6523	1.2873	1.65232	1.28732	1.65235	1.28726
5	–	–	–	–	2.39026	2.15024	2.39014	2.15053

5. Concluding remarks

Numerical solution for MHD Maxwell nanofluid with gyrotactic microorganisms, a higher-order chemical reaction in the presence of variable source/sink, and Newtonian heating is investigated in a rotating flow on a deformable surface. The flow is analyzed with additional effect of Darcy Forchheimer flow amalgamated with modified Fourier and Fick laws. Numerical solution of the flow model is computed via bvp4c function in MATLAB. The following are the notable outcomes of the current investigation:

- Fluid velocity deteriorates on incrementing the rotation parameter.
- On escalating fluid relaxation time $f'(\zeta)$ declines, whereas, for $j(\zeta)$ opposite outcome is observed.
- By augmenting the conjugate heat parameter $\theta(\zeta)$ amplifies.
- For larger values of higher order chemical reaction solutal field escalates.
- For higher estimation of Peclet number, the motile density deteriorates.
- On incrementing the conjugate heat parameter and thermal relaxation time rate of heat transfer augments.
- The rate of heat transfer decreases on varying the fluid relaxation time.

Conflict of interest

The authors have no conflict of interest regarding this publication.

7. Author contribution statement

M.R. supervised and conceived the idea; N.S wrote the manuscript; J.D.C. & S.K. did the software work; Y.M.C. did funding arrangements; F.W. helped in graphical depiction; M.Y.M. and H. A.S.G. helped in revising the manuscript.

Acknowledgments

The authors extend their appreciation to the Deanship of Scientific Research at King Khalid University, Abha 61413, Saudi Arabia for funding this work through research groups program under Grant Number R.G.P-1/88/42.

References

Crane, L.J., 1970. Flow past a stretching plate. Zeitschrift für angewandte Mathematik und Physik ZAMP 21 (4), 645–647.
Sreedevi, P., Reddy, P.S., 2020. Combined influence of Brownian motion and thermophoresis on Maxwell three-dimensional nanofluid flow over stretching sheet with chemical reaction and thermal radiation. J. Porous Media 23 (4), 327–340.
Hussain, S.M., Sharma, R., Mishra, M.R., Alrashidy, S.S., 2020. Hydromagnetic dissipative and radiative graphene Maxwell nanofluid flow past a stretched sheet-numerical and statistical analysis. Mathematics 8 (11), 1929.
Ali, A., Shehzadi, K., Sulaiman, M., Asghar, S., 2019. Heat and mass transfer analysis of 3D Maxwell nanofluid over an exponentially stretching surface. Phys. Scr. 94 (6), 065206.
Prabhavathi, B., Sudarsana Reddy, P., Bhuvana Vijaya, R., 2018. Heat and mass transfer enhancement of SWCNTs and MWCNTs based Maxwell nanofluid flow over a vertical cone with slip effects. Powder Technol. 340, 253–263.
Kundu, P.K., Chakraborty, T., Das, K., 2018. Framing the Cattaneo-Christov heat flux phenomena on CNT-based Maxwell Nanofluid along stretching sheet with multiple slips. Arab. J. Sci. Eng. 43 (3), 1177–1188.
Aziz, A., Muhammad, T., Hayat, T., Alsaedi, A., 2019. Influence of homogeneous–heterogeneous reactions in the three-dimensional rotating flow of a nanofluid subject to Darcy-Forchheimer porous medium: an optimal analysis. Phys. Scr. 94 (11), 115708.
Shah, Z., Tassaddiq, A., Islam, S., Alklaibi, A.M., Khan, I., 2019. Cattaneo-Christov heat flux model for three-dimensional rotating flow of SWCNT and MWCNT nanofluid with Darcy-Forchheimer porous medium induced by a linearly stretchable surface. Symmetry 11 (3), 331.
O. Alzahrani, E., Shah, Z., Alghamdi, W., Zaka Ullah, M., 2019. Darcy-forchheimer radiative flow of micropoler CNT nanofluid in rotating frame with convective heat generation/consumption. Processes 7 (10), 666. https://doi.org/10.3390/pr7100666.
Ullah, M.Z., Alshomrani, A.S., Alghamdi, M., 2020. Significance of Arrhenius activation energy in Darcy-Forchheimer 3D rotating flow of nanofluid with radiative heat transfer. Physica A 550, 124024.
Hayat, T., Aziz, A., Muhammad, T., Alsaedi, A., 2019. Numerical simulation for Darcy-Forchheimer three-dimensional rotating flow of nanofluid with prescribed heat and mass flux conditions. J. Therm. Anal. Calorim. 136 (5), 2087–2095.
Shafiq, A., Rasool, G., Khalique, C.M., 2020. Significance of thermal slip and convective boundary conditions in three dimensional rotating Darcy-Forchheimer nanofluid flow. Symmetry 12 (5), 741.
Ramaiah, K.D., P., S., Kotha, G., Thangavelu, K., 2020. MHD rotating flow of a Maxwell fluid with Arrhenius activation energy and non-Fourier heat flux model. Heat Transfer 49 (4), 2209–2227.
Hayat, T., Aziz, A., Muhammad, T., Alsaedi, A., 2020. Significance of homogeneous–heterogeneous reactions in Darcy-Forchheimer three-dimensional rotating flow of carbon nanotubes. J. Therm. Anal. Calorim. 139 (1), 183–195.
Thumma, T., Mishra, S.R., 2020. Effect of nonuniform heat source/sink, and viscous and Joule dissipation on 3D Eyring-Powell nanofluid flow over a stretching sheet. J. Comput. Design Eng.
Jakati, S.V., Raju, B.T., Nargund, A.L., Sathyanarayana, S.B., 2019. Study of Maxwell Nanofluid flow over a stretching sheet with non-uniform heat source/sink with external magnetic field. J. Adv. Res. Fluid Mech. Thermal Sci. 55, 218–232.
Kumar, K.A., Sugunamma, V., Sandeep, N., Mustafa, M.T., 2019. Simultaneous solutions for first order and second order slips on micropolar fluid flow across a convective surface in the presence of Lorentz force and variable heat source/sink. Sci. Rep. 9 (1), 1–14.
Khan, A., Shah, Z., Islam, S., Khan, S., Khan, W., Khan, A. Z. (2018). Darcy–Forchheimer flow of micropolar nanofluid between two plates in the rotating frame with non-uniform heat generation/absorption. Adv. Mech. Eng., 10(10), 1687814018808850.
Abbasi, A., Farooq, W., Riaz, I., 2020. Stagnation point flow of Maxwell nanofluid containing gyrotactic micro-organism impinging obliquely on a convective surface. Heat Transfer 49 (5), 2977–2999.
Ahmad, I., Aziz, S., Ali, N., Ullah Khan, S., Ijaz Khan, M., Tlili, I., Khan, N.B., 2020. Thermally developed Cattaneo-Christov Maxwell nanofluid over bidirectional periodically accelerated surface with gyrotactic microorganisms and activation energy. Alexandria Eng. J. 59 (6), 4865–4878.
Khan, M.N., Nadeem, S., 2020. Theoretical treatment of bio-convective Maxwell nanofluid over an exponentially stretching sheet. Can. J. Phys. 98 (8), 732–741.
Sohail, M., Naz, R., Abdelsalam, S.I., 2020. On the onset of entropy generation for a nanofluid with thermal radiation and gyrotactic microorganisms through 3D flows. Phys. Scr. 95 (4), 045206. https://doi.org/10.1088/1402-4896/ab3c3f.
Narender, G., Govardhan, K., Sarma, G. S. (2020). Convection of Maxwell nanofluid with the effects of viscous dissipation and chemical reaction over a stretching sheet. In AIP Conference Proceedings (Vol. 2246, No. 1, p. 020052). AIP Publishing LLC.
Ibrahim, W., Negera, M., 2020. MHD slip flow of upper-convected Maxwell nanofluid over a stretching sheet with chemical reaction. J. Egypt. Math. Soc. 28 (1), 7.
Ijaz Khan, M., Nasir, T., Hayat, T., Khan, N.B., Alsaedi, A., 2020. Binary chemical reaction with activation energy in rotating flow subject to nonlinear heat flux and heat source/sink. J. Comput. Des. Eng.
Khan, M., Malik, M.Y., Salahuddin, T., Khan, F., 2019. Generalized diffusion effects on Maxwell nanofluid stagnation point flow over a stretchable sheet with slip conditions and chemical reaction. J. Braz. Soc. Mech. Sci. Eng. 41 (3), 138.

Ramzan, M., Yousaf, F., 2015. Boundary layer flow of three-dimensional viscoelastic nanofluid past a bi-directional stretching sheet with Newtonian heating. AIP Adv. 5 (5), 057132. https://doi.org/10.1063/1.4921312.

Xia, W.-F., Animasaun, I.L., Wakif, A., Shah, N.A., Yook, S.-J., 2021. Gear-generalized differential quadrature analysis of oscillatory convective Taylor-Couette flows of second-grade fluids subject to Lorentz and Darcy-Forchheimer quadratic drag forces. Int. Commun. Heat Mass Transfer 126, 105395.

Wakif, A., Animasaun, I. L., Sehaqui, R. (2021). A Brief Technical Note on the Onset of Convection in a Horizontal Nanofluid Layer of Finite Depth via Wakif-Galerkin Weighted Residuals Technique (WGWRT). In Defect and Diffusion Forum (Vol. 409, pp. 90-94). Trans Tech Publications Ltd.

Rasool, G., Wakif, A., 2021. Numerical spectral examination of EMHD mixed convective flow of second-grade nanofluid towards a vertical Riga plate using an advanced version of the revised Buongiorno's nanofluid model. J. Therm. Anal. Calorim. 143 (3), 2379–2393.

Wakif, A., Chamkha, A., Thumma, T., Animasaun, I.L., Sehaqui, R., 2021. Thermal radiation and surface roughness effects on the thermo-magneto-hydrodynamic stability of alumina–copper oxide hybrid nanofluids utilizing the generalized Buongiorno's nanofluid model. J. Therm. Anal. Calorim. 143 (2), 1201–1220.

Wakif, A., Chamkha, A., Animasaun, I.L., Zaydan, M., Waqas, H., Sehaqui, R., 2020. Novel physical insights into the thermodynamic irreversibilities within dissipative EMHD fluid flows past over a moving horizontal riga plate in the coexistence of wall suction and joule heating effects: a comprehensive numerical investigation. Arab. J. Sci. Eng. 45 (11), 9423–9438.

Alghamdi, M., Wakif, A., Thumma, T., Khan, U., Baleanu, D., Rasool, G., 2021. Significance of variability in magnetic field strength and heat source on the radiative-convective motion of sodium alginate-based nanofluid within a Darcy-Brinkman porous structure bounded vertically by an irregular slender surface. Case Studies. Therm. Eng. 28, 101428. https://doi.org/10.1016/j.csite.2021.101428.

Thumma, T., Wakif, A., Animasaun, I. L. (2020). Generalized differential quadrature analysis of unsteady three-dimensional MHD radiating dissipative Casson fluid conveying tiny particles. Heat Transfer, 49(5), 2595-2626.

Shaheen, N., Ramzan, M., Alshehri, A., Shah, Z., Kumam, P., 2021. Soret-Dufour impact on a three-dimensional Casson nanofluid flow with dust particles and variable characteristics in a permeable media. Sci. Rep. 11 (1), 1–21.

Wakif, A., Sehaqui, R. (2020). Generalized differential quadrature scrutinization of an advanced MHD stability problem concerned water-based nanofluids with metal/metal oxide nanomaterials: a proper application of the revised two-phase nanofluid model with convective heating and through-flow boundary conditions. Numerical Methods for Partial Differential Equations.

Chen, S.B., Shahmir, N., Ramzan, M., Sun, Y.L., Aly, A.A., Malik, M.Y., 2021. Thermophoretic particle deposition in the flow of dual stratified Casson fluid with magnetic dipole and generalized Fourier's and Fick's laws. Case Studies Thermal Eng. 26, 101186.

Nazar, R., Amin, N., Pop, I., 2004. Unsteady boundary layer flow due to a stretching surface in a rotating fluid. Mech. Res. Commun. 31 (1), 121–128.

Wang, C.Y., 1988. Stretching a surface in a rotating fluid. Zeitschrift für angewandte Mathematik und Physik ZAMP 39 (2), 177–185.

Ali, B., Nie, Y., Hussain, S., Manan, A., Sadiq, M.T., 2020. Unsteady magneto-hydrodynamic transport of rotating Maxwell nanofluid flow on a stretching sheet with Cattaneo-Christov double diffusion and activation energy. Thermal Sci. Eng. Prog. 20, 100720.